

2 Structure of Solid Matter

When atoms are chemically bound to one another they have well-defined equilibrium separations that are determined by the condition that the total energy is minimized. Therefore, in a solid composed of many identical atoms, the minimum energy is obtained only when every atom is in an identical environment. This leads to a three-dimensional periodic arrangement that is known as the crystalline state. The same is true for solids that are composed of more than one type of element. In this case, certain “building blocks” comprising a few atoms are the periodically repeated units. Periodicity gives rise to a number of typical properties of solids. Periodicity also simplifies the theoretical understanding and the formal theory of solids enormously. Although a real solid never possesses exact three-dimensional periodicity, one assumes perfect periodicity as a model and deals with the defects in terms of a perturbation (Sect. 2.7). Three-dimensional periodic arrangements of atoms or “building blocks” are realized in many different ways. Basic elements of the resulting crystal structures are described in Sects. 2.1–2.5.

The counterpart to the crystalline state of solids is the amorphous state. This is a state in which no long-range order exists; however, a degree of short-range order remains. Examples of amorphous solids are glasses, ceramics, gels, polymers, rapidly quenched melts and thin-film systems deposited on a substrate at low temperatures. The investigation of amorphous materials is a very active area of research. Despite enormous progress in recent years, our understanding of amorphous materials still remains far from complete. The reason is the absence of the simplifications associated with periodicity. Nonetheless, from comparison of the properties of materials in a crystalline and an amorphous state we have learned the essential features of the electronic structure, and thereby also macroscopic properties, are determined by short-range order. Thus these properties are similar for solids in the amorphous and crystalline state. In the context of this book we focus on a few structural and electronic properties of amorphous solid in Sects. 3.1, 7.6 and 9.8.

Materials of practical use are nearly always composites. Examples, some of them known to mankind since early ages, are the bronzes (alloys of copper and tin), brass (copper and zinc) or steel (in its simplest form iron with a few per cent of carbon). Modern material science has supplemented these classical, mostly binary alloys with many multi-component systems including composite materials. In the framework of this textbook,

particular attention will be paid to semiconductor alloys (Chap. 12). Alloys typically do not exist as a homogenous crystalline phase; they rather consist of microcrystallites, whose composition depends on temperature, pressure, and the percentage of the constituting elements. Phase diagrams of simple binary alloys are discussed in Sect. 2.6.

2.1 The Crystal Lattice

A two-dimensional lattice is spanned by two vectors \mathbf{a} and \mathbf{b} . Every point on the lattice can be reached by a lattice vector of the form

$$\mathbf{r}_n = n_1 \mathbf{a} + n_2 \mathbf{b} \quad (2.1)$$

where n_1 and n_2 are integers. Depending on the ratio of the lengths of the vectors \mathbf{a} and \mathbf{b} , and on the angle γ between them, lattices of various geometries can be constructed. The most general lattice, with no additional symmetry, is obtained when $a \neq b$ and $\gamma \neq 90^\circ$ (Fig. 2.1). A planar crystal structure would be produced if every point of this “parallelogram lattice” were occupied by one atom. In this case, each elementary (or unit) cell with sides \mathbf{a} and \mathbf{b} would contain one atom. Such elementary cells are termed primitive. It is also possible for crystal structure to contain more than one atom per unit cell. In such cases the lattice points of Fig. 2.1 correspond to points in the crystal which all have identical environments. Such points may, but need not necessarily, lie at the center of an atom.

Other planar lattices of higher symmetry are obtained when γ , a and b take on certain special values. The rectangular lattice is obtained when $\gamma = 90^\circ$ (Fig. 2.2). When additionally $a = b$, this becomes a square lattice. The two-dimensional plane can also be filled with a regular array of hexagons. The unit cell is then given by $a = b$ and $\gamma = 60^\circ$. A hexagonal close packing of spheres has this unit cell. The condition $a = b$ with γ arbitrary also produces a new type of lattice. However, this lattice is more conveniently described as a “centered” rectangular lattice with $a \neq b$ and $\gamma = 90^\circ$ (Fig. 2.2). One thereby obtains the advantage of an orthogonal coordinate system; the lattice, however, is no longer primitive.

It is easy to see that the description in terms of a centered unit cell is only useful for a rectangular lattice. If centering is introduced into a square, parallelogram or hexagonal lattice, it is always possible to describe

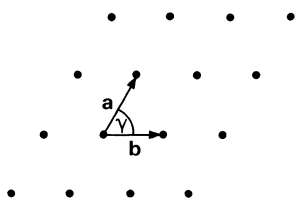


Fig. 2.1. A plane oblique lattice

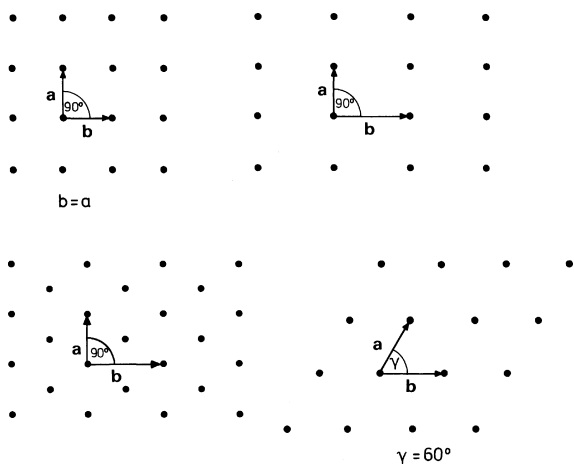


Fig. 2.2. Further two-dimensional lattices: square, rectangular, centered rectangular and hexagonal ($\gamma = 60^\circ$, $a = b$)

the new lattice in terms of an alternative set of smaller basis vectors. In other words, the only result is that one has obtained a larger than necessary unit cell.

The discussion so far has concerned two-dimensional lattices, but the principles can be extended to lattices in three dimensions. Instead of the five possible systems of basis vectors in the plane, one now has seven possibilities (Table 2.1). These correspond to the seven distinct crystal systems of crystallography. With the addition of centering, one can construct from these basis vector systems all the possible lattices of three-dimensional space. As well as face centering, one now has the additional possibility of body centering (Fig. 2.3). As was the case in two dimensions, one can readily convince oneself that only certain

Table 2.1. The seven different basis-vector systems or crystal systems. Most elements crystallize in a cubic or hexagonal structure. For this reason, and also because of their high symmetry, the cubic and hexagonal coordinate systems are particularly important

Basis vectors/crystal axes	Angles	Crystal system
$a \neq b \neq c$	$\alpha \neq \beta \neq \gamma \neq 90^\circ$	triclinic
$a \neq b \neq c$	$\alpha = \gamma = 90^\circ \beta \neq 90^\circ$	monoclinic
$a \neq b \neq c$	$\alpha = \beta = \gamma = 90^\circ$	orthorhombic
$a = b \neq c$	$\alpha = \beta = \gamma = 90^\circ$	tetragonal
$a = b \neq c$	$\alpha = \beta = 90^\circ \gamma = 120^\circ$	hexagonal
$a = b = c$	$\alpha = \beta = \gamma \neq 90^\circ$	rhombohedral
$a = b = c$	$\alpha = \beta = \gamma = 90^\circ$	cubic

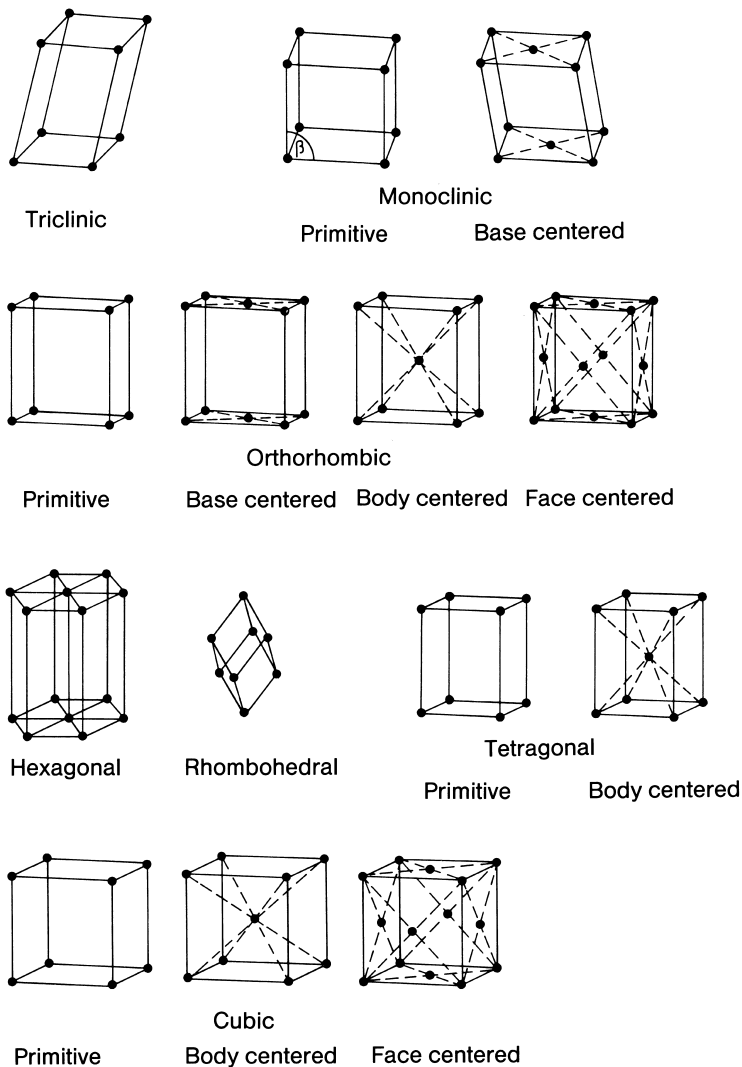


Fig. 2.3. The 14 three-dimensional Bravais lattices. The hexagonal lattice and the two centered cubic lattices are particularly important in solid state physics

centerings are useful. For example, it would not make sense to employ a tetragonal base-centered lattice because this is equivalent to a primitive tetragonal lattice with a smaller unit cell.

2.2 Point Symmetry

Every point of the lattices just discussed represents an atom, or a more-or-less complicated group of atoms, each of which has particular symmetry properties. The symmetries and the corresponding notation will be presented in the following.

Reflection in a Plane

This symmetry is expressed mathematically by a coordinate transformation. For example, mirror symmetry about the yz -plane is represented by the transformation $y' = y$, $z' = z$, $x' = -x$. The presence of a mirror plane in a crystal structure is indicated by the symbol m . An example of a molecule possessing two perpendicular mirror planes is the water molecule (Fig. 2.7). One of the mirror planes is the plane defined by the atoms of the molecule; the other is perpendicular to this and passes through the oxygen atom, bisecting the molecule.

Inversion

Inversion symmetry is described by the coordinate transformation $x' = -x$, $y' = -y$, $z' = -z$. Thus in a sense this might be described as reflection in a point. The symbol representing inversion symmetry is $\bar{1}$. An example of a molecule possessing inversion symmetry is cyclohexane (Fig. 2.4). Homonuclear diatomic molecules also have inversion symmetry and, of course, mirror planes.

Rotation Axes

Rotational symmetry is present if a rotation through a particular angle about a certain axis, leads to an identical structure. The trivial case is, of

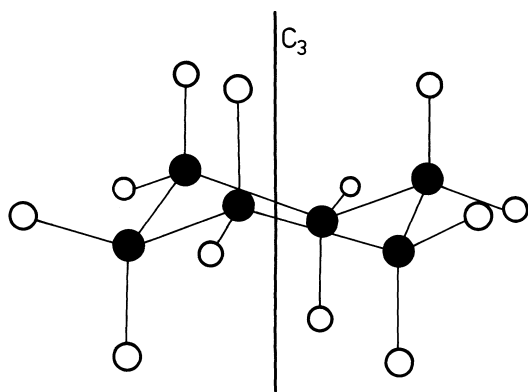


Fig. 2.4. The cyclohexane molecule (C_6H_{12}). The principal symmetry element is the 3-fold axis of rotation C_3 . The molecule also has a center of inversion, three mirror planes and, perpendicular to the main axis, three 2-fold rotation axes at 120° to one another. The point group is denoted by D_{3d} (Table 2.2)

course, rotation by 360° which inevitably leads to the same structure. The number of intermediate rotations that also result in indistinguishable arrangements is called “the order” of the rotation axis. Thus one can have 2-, 3-, 4- and 6-fold rotation axes, corresponding to invariance under rotations of 180° , 120° , 90° , and 60° . For single molecules it is also possible to have 5-fold, 7-fold, etc., axes. Small solid aggregates (clusters) may also display 5-fold rotational symmetry. An example is the particularly stable icosahedron composed of 13 atoms. Icosahedra are formed in the rapid quenching of melts. The solid which is thus formed has a quasi crystalline structure and produces sharp X-ray diffraction spots that reflect the local 5-fold symmetry [2.1]. For strictly periodic crystals, however, only 2-, 3-, 4- and 6-fold rotation axes are possible. All other orders of rotation are incompatible with the required translational symmetry. The notation describing the possible axes of rotation is given simply by the numbers 2, 3, 4 and 6.

The cyclohexane molecule shown in Fig. 2.4 has a 3-fold rotation axis. A molecule with a 6-fold axis is benzene (C_6H_6), whose carbon skeleton consists of a planar regular hexagon.

Rotation-Inversion Axes

Rotation with simultaneous inversion can be combined to give a new symmetry element – the rotation-inversion axis. It is symbolized by $\bar{2}$, $\bar{3}$, $\bar{4}$, or $\bar{6}$. Figure 2.5 illustrates a 3-fold rotation-inversion axis. From this it is evident that a 3-fold rotation-inversion axis is equivalent to a 3-fold rotation together with inversion. The 6-fold rotation-inversion axis may alternatively be represented as a 3-fold rotation axis plus a mirror plane.

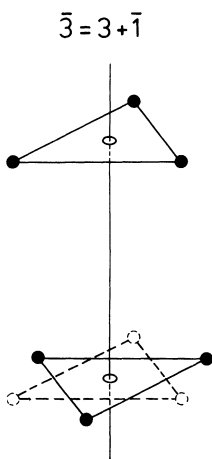


Fig. 2.5. Representation of a 3-fold rotation-inversion axis. The effect can also be described by the combination of other symmetry elements

2.3 The 32 Crystal Classes (Point Groups)

The symmetry elements discussed in the previous section may be combined with one another in various ways. Conversely, every crystal may be described by a particular combination of point-symmetry elements. To be complete, the description must satisfy a number of conditions. For example, if two successive symmetry operations are applied, the result must be a further symmetry element: $A \otimes B = C$. Three (or more successive symmetry operations must obey the so-called associativity rule: $(A \otimes B) \otimes C = A \otimes (B \otimes C)$. There is an identity element E , corresponding to no operation or to a rotation about 360° , such that $A \otimes E = A$. Furthermore, every symmetry element A possesses an inverse A^{-1} , which corresponds to the reverse operation, so that $A^{-1} \otimes A = E$. These properties are the mathematical definition of a group. There are 32 distinct crystallographic point groups. If the translational symmetry is also taken into account then one obtains the 230 possible space groups. Although not necessarily true in general, we should note that for translations $A \otimes B = B \otimes A$ (the property of Abelian groups).

The 32 crystallographic point groups are most commonly represented by so-called stereographic projections. These projections were developed by crystallographers in order to obtain a systematic classification of the exposed surfaces of naturally grown crystals. The point at which each surface normal intersects a sphere is marked and then projected onto the plane perpendicular to the highest order symmetry axis. Intersection points above this plane are marked by a full circle, and those on the lower half sphere by an open circle or a cross. Hence, in the systematic representation of the point groups, the highest order axis lies in the center. Stereographic projections of two point groups are shown in Fig. 2.6. A particular point group may be denoted in three different ways:

- 1) by specifying a system of generating symmetry operations;
- 2) by specifying the international point group symbol;
- 3) by the Schönflies symbol.

The notation based on the generating symmetry operators is common in crystallography, whereas the Schönflies symbols have largely been adopted in group theory and spectroscopy. The Schönflies notation consists of a

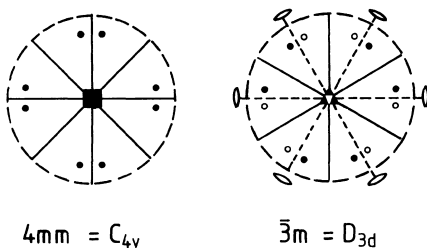


Fig. 2.6. Representation in stereographic projection of the symmetry elements of two point groups. The symbols \circ , \triangle , and \blacksquare denote 2-, 3-, and 4-fold rotation axes. The full lines are mirror planes. When the outer circle is also drawn as a full line, this indicates that the plane of the drawing is also a mirror plane

Table 2.2. The Schönflies point group symbols

	Symbol	Meaning
Classification according to rotation axes and principal mirror planes	C_j	($j = 2, 3, 4, 6$) j -fold rotation axis
	S_j	j -fold rotation-inversion axis
	D_j	j two-fold rotation axes \perp to a (j -fold) principal rotation axis
	T	4 three- and 3 two-fold rotation axes as in a tetrahedron
	O	4 three- and 3 four-fold rotation axes as in an octahedron
	C_i	a center of inversion
Additional symbols for mirror planes	C_s	a mirror plane
	h	horizontal = perpendicular to the rotation axis
	v	vertical = parallel to the main rotation axis
	d	diagonal = parallel to the main rotation axis in the plane bisecting the 2-fold rotation axes

main symbol that characterizes the axes of rotation (if any) of the system, and a subsidiary symbol that gives the positions of the symmetry planes. The symbols and their meanings are summarized in Table 2.2. As an example, we consider the water molecule, for which the highest order rotation axis is a 2-fold axis. The symmetry planes are vertical, i.e. they lie parallel to the main axis of rotation. The corresponding Schönflies symbol is C_{2v} . A cube has three 4-fold rotation axes, four 3-fold rotation axes and symmetry planes perpendicular to the 4-fold axes. Its Schönflies symbol is O_h .

2.4 The Significance of Symmetry

To the uninitiated, the correct assignment and symbolization of symmetry often seems complicated and confusing. It will thus be useful to give a brief overview of the importance of symmetry in the description of a solid. For this purpose, we base our discussion on quantum mechanics. As we have seen, the water molecule, for example, has two mirror planes. The presence of these two mirror planes must somehow be reflected in all the physical properties of the molecule. When the electronic or vibrational properties of the molecule are described by a Hamiltonian, then this has 2-fold mirror symmetry, i.e., it remains invariant under the corresponding coordinate transformation. This invariance can also be expressed in other ways. An operator σ is assigned to the reflection. When σ operates on the Hamiltonian \mathcal{H} , on an eigenstate ψ or on \mathbf{R} , the result should describe \mathcal{H} , ψ or \mathbf{R} in the transformed (mirror image) coordinates.

Such operators are represented as matrices. Thus the reflection of coordinates in the yz -plane is represented by the matrix operation

$$\begin{pmatrix} -1 & 0 & 0 \\ 0 & 1 & 0 \\ 0 & 0 & 1 \end{pmatrix} \begin{pmatrix} x \\ y \\ z \end{pmatrix} = \begin{pmatrix} -x \\ y \\ z \end{pmatrix}. \quad (2.2)$$

This is a three-dimensional representation. The same operation can also be expressed in terms of three one-dimensional matrices,

$$[(-1)x; (1)y; (1)z] = (-x; y; z),$$

each of which acts on only one coordinate component. In this case the three-dimensional representation is known as “reducible”, whereas the corresponding one-dimensional representation is called “irreducible” since it cannot be further simplified. It is easy to see that the irreducible representation of a rotation through 180° (a 2-fold rotation axis) is also one-dimensional: for a suitable choice of coordinates, it can be expressed simply by a sign reversal. However, for 3-, 4- and 6-fold rotation axes, except for the case of a 360° rotation, the operations always involve two coordinate changes. The irreducible representation is therefore two-dimensional.

If the Hamiltonian operator possesses a particular symmetry, for example mirror symmetry, then it makes no difference whether the reflection operation appears before or after the Hamiltonian operator, i.e., the two operators commute. As is well known from quantum mechanics, such operators have a common set of eigenstates. Thus the possible eigenstates of \mathcal{H} can be classified according to their eigenvalues with respect to the symmetry operators. In the case of mirror symmetry and that of a 2-fold rotation axis C_2 , one has $\sigma^2 = 1$ and $C_2^2 = 1$ and thus the eigenvalues can only be ± 1 :

$$\begin{aligned} \sigma \Psi_+ &= +\Psi_+, & C_2 \Psi_+ &= +\Psi_+, \\ \sigma \Psi_- &= -\Psi_-, & C_2 \Psi_- &= -\Psi_-. \end{aligned} \quad (2.3)$$

The eigenstates of \mathcal{H} may therefore be either symmetric or antisymmetric with respect to these operators. This is often expressed by saying that the eigenstates have even or odd “parity”. We have already met an example of even and odd parity in our discussion of the chemical bonding between hydrogen atoms (Sect. 1.2). The bonding state was a symmetric combination of atomic wavefunctions and therefore a state of even parity. As seen in this example, the eigenstates Ψ_+ and Ψ_- belong to distinct eigenvalues of \mathcal{H} . The corresponding energy levels are thus nondegenerate. From this we may conclude, for example, that the water molecule can possess only nondegenerate energy states (we ignore here any accidental degeneracy of energy levels or normal mode vibrations).

To illustrate the above discussion we will apply these ideas to the normal mode vibrations of the water molecule. Accordingly, the atoms can move symmetrically or antisymmetrically with respect to the two mirror planes of the molecule. For atoms that lie in a mirror plane, antisymmetric motion with respect to the plane implies motion perpendicular to the plane, since only then can reflection reverse the motion. The corresponding sym-

metric vibrations of such atoms must involve motion in the mirror plane. One of the two mirror planes of the H_2O molecule is the plane containing the three atoms (Fig. 2.7). The motions that are antisymmetric with respect to this plane are two rotations of the molecule and its translation perpendicular to the plane. The six symmetric modes with motion in the plane of the molecule are two translations, a rotation about an axis perpendicular to the plane, and the three normal mode vibrations (Fig. 2.7). Of these vibrations two are symmetric and one is antisymmetric with respect to the mirror plane *perpendicular* to the molecular plane.

For more complex molecules too, it is possible to perform such a classification of the vibrational modes and/or electronic states. However, the process becomes rather more involved for operators that have two-dimensional irreducible representations, such as C_3 . If C_3 commutes with \mathcal{H} , then together with the state Ψ , the state $C_3\Psi$ is also an eigenstate of \mathcal{H} . There are now two possibilities:

- 1) Apart from a numerical factor, which, for suitable normalization can be made equal to 1, the state $C_3\Psi$ is identical to Ψ . Thus, in this case Ψ is totally symmetric with respect to C_3 and the operation C_3 has a one-dimensional (numerical) representation. The state Ψ is then – at least with respect to the operation – nondegenerate.
- 2) $C_3\Psi$ produces a new, linearly independent state Ψ' , which however, due to the commutivity of C_3 and \mathcal{H} , must also be an eigenstate of \mathcal{H} with the same eigenvalue E . The states Ψ and Ψ' are thus degenerate. Since the rotation C_3 always affects two coordinates, its irreducible representation is a two-dimensional matrix. Every eigenstate of C_3 may then be constructed as a linear combination of two functions that

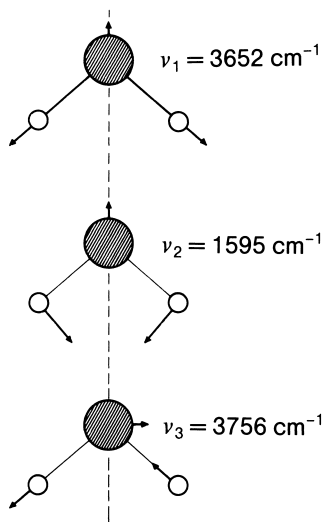


Fig. 2.7. The two symmetric and the antisymmetric vibrations of the water molecule. Together with the three rotations and three translations these give the nine normal modes corresponding to the nine degrees of freedom

can be selected to be orthonormal. The energy levels are therefore 2-fold degenerate. Such degenerate levels are found for all point groups possessing more than a 2-fold rotation axis.

Particularly important in solid state physics are the diamond lattice and the face-centered and body-centered cubic lattices. These belong to the point groups T_d and O_h , respectively, the former displaying tetrahedral and the latter octahedral symmetry (Figs. 2.8, 10, 12). The representations of such symmetries affect three coordinates and thus T_d and O_h have three-dimensional irreducible representations. They are associated accordingly with 3-fold degeneracy. We will meet such states when we deal with the normal modes of these lattices (Sect. 4.5) and their electron states (Sect. 7.4).

Besides symmetry-determined degeneracy, one also finds degeneracy that results from the specific form of \mathcal{H} . The degeneracy associated with the angular momentum quantum number l of the hydrogen atom is well known to be a result of the $1/r$ potential, whereas the degeneracy with respect to the magnetic quantum number m stems from symmetry. The crystal symmetry also determines the number of independent components of the tensors describing macroscopic material properties. We note here for later use that second-rank tensors, such as the thermal expansion or susceptibility, have only one independent component in cubic crystals, and two in hexagonal crystals. The symmetry of the fourth rank elastic tensor is discussed in Sect. 4.5.

2.5 Simple Crystal Structures

The Face-Centered Cubic Structure

The simplest crystal structures are those in which each point of the lattice is occupied by one atom. In this case, the face-centered cubic lattice produces a face-centered cubic crystal. Each atom in this structure is surrounded by 12 nearest neighbors. The number of nearest neighbors in a particular structure type is known as the coordination number.

The coordination number 12 represents the highest possible packing density for spheres. In a single plane of close-packed spheres the number of nearest neighbors is 6. In three dimensions there are an additional 3 nearest neighbors in each of the planes below and above. If the lattice constant of the face-centered structure is denoted by a , then the separation of nearest neighbors is given by $a/\sqrt{2}$ as is readily seen from Fig. 2.8. The closest-packed planes are sketched in Fig. 2.8b. They lie perpendicular to the main diagonal of the cube. If one moves away from a particular close-packed plane along the main diagonal, another identical plane is reached only after passing through two differently positioned close-packed planes. This packing sequence is illustrated more clearly by Fig. 2.9. A close-packed layer has two sorts of hollow sites (visible in layer A). The second layer is obtained by placing further spheres on one of the two possible sites, and the third-

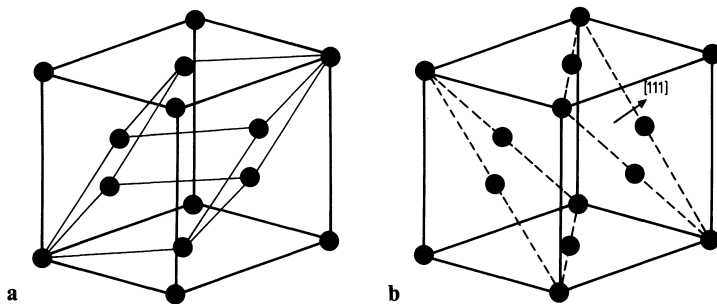


Fig. 2.8 a, b. The face-centered cubic structure showing the primitive rhombohedral unit cell (a). The close-packed planes are illustrated by dotted lines in (b). The number of nearest neighbors (the coordination number) is 12

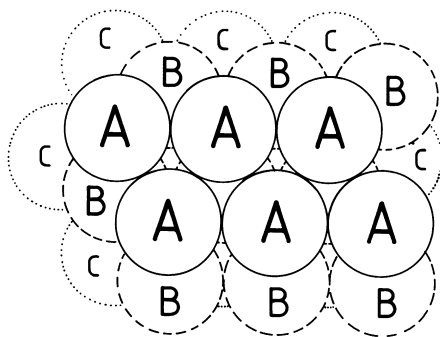


Fig. 2.9. The close-packed layers of the fcc structure with the stacking sequence ABCABC...

layer spheres lie above the other type of site. Thus the face-centered cubic structure is composed of close-packed layers in the stacking sequence ABCABC... . Each of these layers alone has hexagonal (6-fold) symmetry; however, stacked above one another in this manner the symmetry is reduced to a 3-fold rotation axis (Fig. 2.9). The face-centered cubic structure therefore has four 3-fold rotation axes as well as a mirror plane perpendicular to the 4-fold axis. It therefore belongs to the point group O_h . The face-centered cubic structure is usually denoted by the abbreviation fcc. Examples of fcc crystals are the metals Cu, Ag, Au, Ni, Pd, Pt and Al. Despite their relatively high melting points these metals are fairly soft. The reason for this is that the close-packed layers are able to slide over one another. This sliding motion occurs in the plastic deformation of these crystals. However, it does not involve an entire layer; it is limited to regions associated with dislocations (Sect. 2.7).

Hexagonal Close Packing

The hexagonal close-packed (hcp) structure results when close-packed planes are stacked in the sequence ABAB... . In contrast to the fcc structure, the

smallest possible unit cell now contains two atoms. Thus the main axis of rotation is again 3-fold rather than 6-fold. As can be seen by considering only the layers A and B of Fig. 2.9, there exist three 2-fold rotation axes perpendicular to the 3-fold axis. Furthermore, the close-packed layer also lies in a mirror plane. The point group corresponding to these symmetry elements is D_{3h} . As with the fcc structure, the coordination number is 12. Important metals that crystallize in the hcp structure include Zn, Cd, Be, Mg, Re, Ru and Os.

The Body-Centered Cubic Structure

The body-centered cubic (bcc) structure is shown in Fig. 2.10. For this structure the coordination number is only 8. Thus for nondirectional bonding the bcc structure would appear to be less favorable. Nonetheless, all alkali metals as well as Ba, V, Nb, Ta, W, and Mo, are found to crystallize in this structure, and Cr and Fe also possess bcc phases. At first sight this is hard to understand. However, it is important to note that in the bcc structure the 6 next-nearest neighbors are only slightly farther away than the 8 nearest neighbors. Thus, depending on the range and the nature of the wavefunctions contributing to the bonding, the effective coordination number of the bcc structure can be higher than that of the fcc structure. Figure 2.11 shows the probability functions for the positions of the lithium electrons relative to the atomic nucleus. Also shown are the half distances to the nearest (r_1), the next-nearest (r_2) and the third-nearest (r_3) neighbors for the actually occurring bcc structure and for a hypothetical fcc structure with the same nearest-neighbor separation. When the next-nearest neighbors are taken into account, it is easy to see that the bcc structure leads to a greater overlap of wavefunctions and thus an increase in the strength of the chemical bonding. This effect is enhanced by the fact that the p -orbitals in a cubic structure are oriented along the edges of the cube, thereby contributing significantly to the bonding with the next-nearest neighbors. The picture

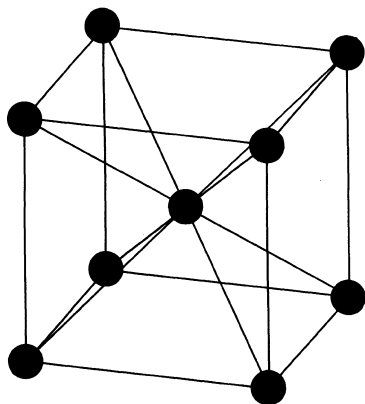


Fig. 2.10. The body-centered cubic structure with coordination number 8

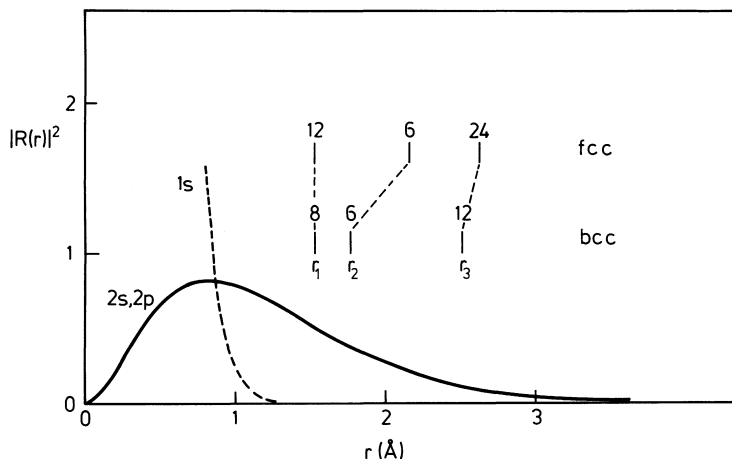


Fig. 2.11. Absolute square of the radial part of the electron wavefunctions of lithium as a function of distance from the nucleus. For the bcc structure, both the 8 nearest and the 6 next-nearest neighbors lie in a region of relatively high density. Hence for non-directional metallic bond it is possible for the bcc structure to be energetically favorable with respect to fcc. Examples of bcc metals are the alkali metals Li, Na, K, Rb, Cs and Fr. This curve may be compared with Fig. 1.9 which shows the wavefunction amplitude rather than the probability density. The decay at large distances then becomes weaker

changes, however, when d -electrons become involved in the bonding. The d -orbitals are directed both along the cube edges and along the diagonals of the faces. Since the d -orbitals are localized relatively strongly on the atoms (Fig. 1.9), they can only contribute to the bonding when they are directed towards the nearest neighbors. The fcc structure enables exactly this, which is the reason why metals with a large number of d -electrons often crystallize in the fcc structure.

The Diamond Structure

The diamond structure belongs to the crystal class T_d . It allows three-dimensional covalent bonding (Sect. 1.2) in which every atom is surrounded by four nearest neighbors in a tetrahedral configuration (Fig. 2.12). Thus the coordination number is 4. The diamond structure takes its name from the structure of the carbon atoms in diamond. Other elements that crystallize with the same structure are Si, Ge and α -Sn. The diamond structure can be described as two interpenetrating fcc structures that are displaced relative to one another along the main diagonal. The position of the origin of the second fcc structure, expressed in terms of the basis vectors, is $(\frac{1}{4}, \frac{1}{4}, \frac{1}{4})$. This leads to a nearest-neighbor distance of $\sqrt{3}a/4$. Since the separation of close-packed layers in the fcc structure is $\sqrt{3}a/3$, the distance of a central atom from the base of its tetrahedron of neighbors is $\frac{1}{4}$ of the total height of the tetrahedron.

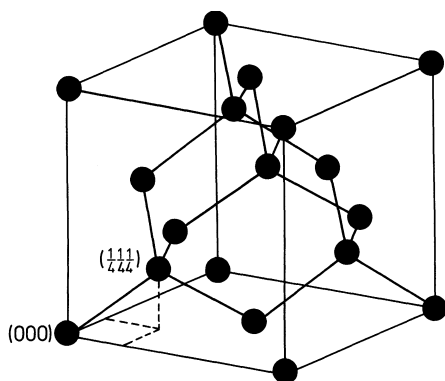


Fig. 2.12. The diamond structure. It consists of two interpenetrating fcc structures which are displaced relative to one another by $1/4$ of the long diagonal of the cube. This type of structure is typical of the elements of group IV of the periodic table (C, Si, Ge, α -Sn) and also for III–V compounds in which the sites (000) and $(\frac{1}{4}, \frac{1}{4}, \frac{1}{4})$ are occupied by different types of atom (ZnS-type structure)

The Zinc Blende Structure

The zinc blende (ZnS) structure is closely related to the diamond structure, but now the two interpenetrating fcc structures contain different atoms. The ZnS structure is found in the most important of the compounds of group III with group V elements. Examples are GaAs, GaP and InSb. The compound ZnS which gives its name to this structure is of course also of the “zinc blende structure”. The choice of name for this structure is actually slightly unfortunate, since the compound ZnS also crystallizes in a hexagonal phase with the so-called wurtzite structure. This structure, in common with the ZnS type, has tetrahedral coordination; however, the stacking sequence of the close-packed (111) planes is no longer ABCABC..., but ABAB..., thereby giving it a hexagonal structure. The wurtzite structure is also adopted by other compounds between group II and group VI elements (ZnO, ZnSe, ZnTe, CdS, CdSe). As well as the ordered packing sequences ABAB... and ABCABC... it is also possible to find mixed forms with random stacking or very long period repeats. The best-known example of these so-called “polytypes” is SiC.

Ionic Structures

Typical ionic structures, exemplified by the CsCl and NaCl structures, have already been introduced in Sect. 1.3 (Fig. 1.6). The CsCl structure is derived from the bcc structure by replacing the ion at the center of the cube by an ion of a different element. The NaCl structure is the result of placing one fcc structure within another. The coordination numbers are 8 for the CsCl structure and only 6 for the NaCl structure. As we have seen in Sect. 1.3, for equal ionic separations, the Madelung constant and thus also the ionic energy are greater for the CsCl structure. Although the differences are relatively small, it is perhaps surprising that the majority of ionic crystals prefer the NaCl structure. The explanation for this is as follows: In most cases, the radius of the cations is much smaller than that of the anion. For example,

$$r_{\text{Na}} = 0.98 \text{ \AA}, \quad r_{\text{Cl}} = 1.81 \text{ \AA}.$$

The cesium ion however is a large cation:

$$r_{\text{Cs}} = 1.65 \text{ \AA}.$$

As the cation becomes smaller, the anions of a CsCl-type structure approach one another and eventually overlap. This occurs at a radius ratio of $r^+/r^- = 0.732$. For still smaller cations the lattice constant could not be further reduced and the Coulomb energy would remain constant. In this case the NaCl-type structure is favored since anion contact does not occur until a radius ratio of $r^+/r^- = 0.414$ is reached. Yet smaller radius ratios are possible for the ZnS-type structure. Indeed, for ZnS itself, the ratio is $r^+/r^- = 0.40$. This can be regarded as the reason why ZnS does not crystallize in the NaCl structure. This is a somewhat simplified view as it neglects the strong covalent contribution to the bonding (see also Problem 1.2).

2.6 Phase Diagrams of Alloys

Modern functional materials consist of many elements in different *phases*. The term *phase* denotes a domain of homogeneous concentration and structure on a length scale that is large compared to atomic dimensions. Separate phases can be observed even with simple binary alloys. Figure 2.13 displays the scanning electron microscope image of the polished surface of an Ag/Cu alloy. The dark and light sections represent copper- and silver-rich fcc-phases, respectively. As a rule, the various constituting phases of modern composite materials are not in thermal equilibrium. Nonetheless,

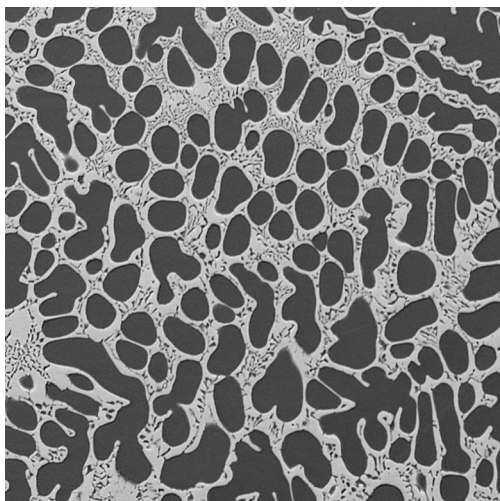


Fig. 2.13. Scanning electron microscope image of a polished specimen of an Ag/Cu alloy with 30% Ag- and 70% Cu-atoms. The dark and light areas consist of fcc-phases with about 95% Cu-atoms and about 86% Ag-atoms, respectively

the equilibrium properties are basic to the understanding. Equilibrium properties are described with the help of *phase diagrams*. In a phase diagram, the temperature is plotted vs. the concentration of one component (at the expense of another). For a particular temperature and composition, the material possesses a particular equilibrium structure. The boundaries between different structures are marked by lines. In the simplest case the lines describe the boundary between the solid and the liquid state. Phase diagrams for all important alloys have been determined experimentally by thermodynamic measurements [2.2]. In the following, we consider only the simple phase diagrams of substitutional binary alloys. A substitutional alloy consists of two types of atoms A and B, which as pure materials crystallize in the same structure. If in addition the chemical bonding is similar and the lattice constants of the pure phases are not too different, atoms A and B will assume the same lattice sites in the composite system. A number of different states exist even in this simple case: the liquid state with a complete mixture of the two components, a mixture of liquid phase and a solid phase in which atoms of either type A or B are enriched, a solid phase with micro-crystals in which either A or B are enriched, or a continuously miscible solid phase. Alloys that are continuously miscible in the solid phase have the simplest phase diagrams. The SiGe alloy is an example. Its phase diagram is displayed in Fig. 2.14. Depending on the temperature and the relative Si-concentration, the alloy exists either as a homogeneous liquid (ℓ for liquidus), as a homogeneous solid (s for solidus) or as a two-phase

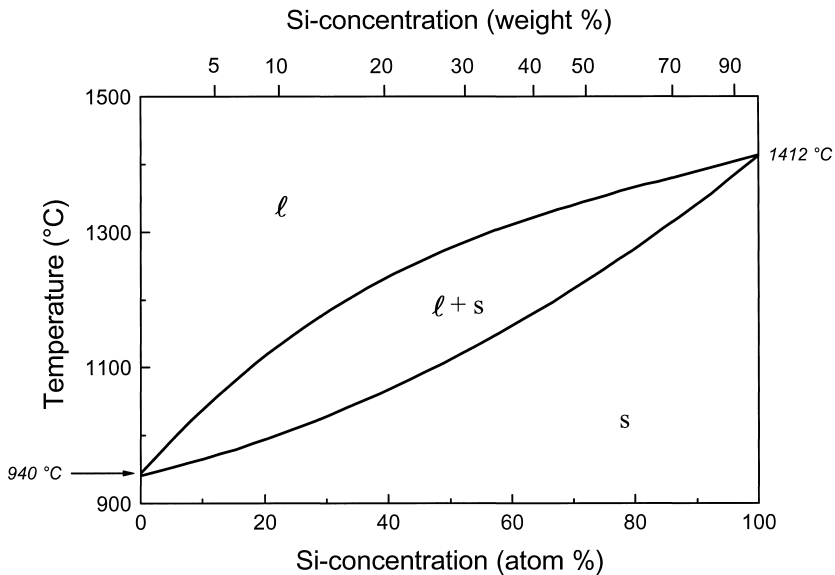


Fig. 2.14. Phase diagram for the continuously miscible alloy Ge/Si. In the range bounded by the liquidus and solidus curves a Ge-rich liquid phase coexists with a Si-rich solid phase

system with liquid and solid parts ($\ell+s$). The realms of existence are marked by the so-called *liquidus* and *solidus* lines. Another substitutional alloy is AgCu. Here, the phase diagram is much more complex (Fig. 2.15). The reason is that the solid phase of AgCu is not completely miscible. Cu is soluble in Ag only up to a particular percentage that depends on the temperature (α -phase, left side of Fig. 2.15). Likewise is Ag in Cu only soluble up to a temperature-dependent percentage (β -phase, right side of Fig. 2.15). In the intermediate range in the so-called *miscibility gap* the solid phase consists of microcrystalline domains of an Ag-rich α -phase and a Cu-rich β -phase (see Fig. 2.13). In real systems, the size and shape of the microcrystals are nearly always determined by kinetics rather than by thermodynamic equilibrium. A defined equilibrium size of the crystallites nevertheless exists. It is determined by the minimum of the interfacial energy between the different crystallites and the elastic strain energy due to the mismatch of the lattice constants between the crystals of different composition. The strain energy decreases as the crystal size becomes smaller. On the other hand the interfacial area and thus the interfacial energy increases so that one has a minimum of the total energy for a particular crystal size.

In the course of this section we want to come to an understanding of the origin of the different phase diagrams of the two substitutional alloys SiGe and AgCu based on thermodynamic reasoning. As seen above, the crucial difference between the two systems is the possibility, respectively impossibility of a continuous mixture in the solid phase. Our thermody-

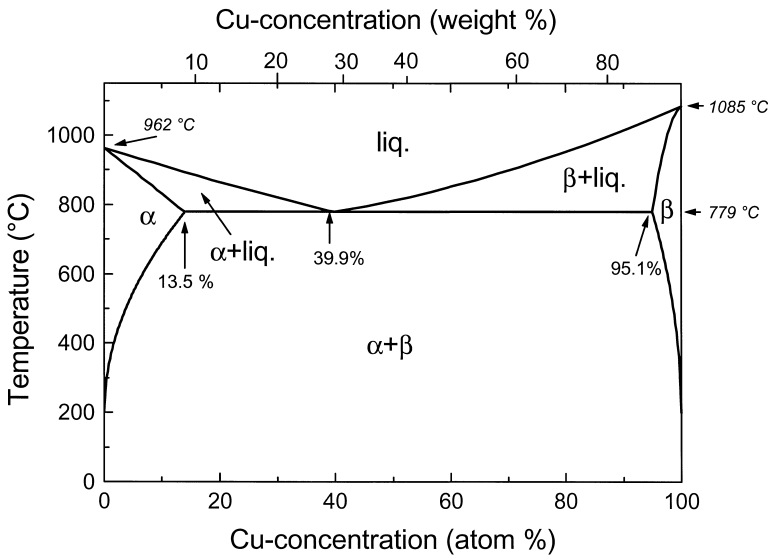


Fig. 2.15. Phase diagram for the binary alloy Ag/Cu. The system is not continuously miscible in the solid phase. Rather the alloy has a wide miscibility gap in which a Ag-rich fcc-phase (α -phase) co-exists with a Cu-rich fcc-phase (β -phase) (see Fig. 2.13)

namic considerations therefore focus on the free enthalpy associated with a mixture. The free enthalpy of a system G is a linear combination comprising of the internal energy U , the entropy S and mechanical (or other) work. In the simple case of a homogeneous, liquid or gaseous matter G is

$$G = U - TS + pV, \quad (2.4)$$

in which T is the temperature, p the pressure and V the volume. In addition to the work against the external pressure one needs to consider the mechanical work associated with the internal degrees of freedom of the system (see discussion above). This part is rather difficult to deal with (see also Sect. 4.5). Fortunately, the contributions of energy and entropy of mixture prevail. We therefore consider only those two contributions in the following and neglect contributions of mechanical, electrical or magnetic work. In a first step we likewise neglect thermal contributions. One further approximation is needed for the purpose of calculating the energy and entropy of mixture: this is that we admit only homogeneously mixed phases, that is we exclude spatial and temporal fluctuations. This corresponds to a *mean field approximation*, an approximation that we encounter quite frequently in the theory of solid matter. In the present context, the approximation is also known as the *Bragg–Williams approximation*. The variation in the enthalpy associated with mixing G_{mix} consists of a variation of the internal energy U_{mix} , which is the heat of solution, and the variation of the entropy due to mixing S_{mix}

$$G_{\text{mix}} = U_{\text{mix}} - TS_{\text{mix}}. \quad (2.5)$$

In a first step we calculate the variation of the internal energy under the assumption that the binding energies of the involved atoms can be represented by nearest neighbor pair interactions. This simple ansatz does not conform with reality but must suffice here. We denote the number of atoms of type A and B as N_A and N_B , and the number of nearest-neighbor bonds between atoms of type A , of type B , and between atoms A and B as N_{AA} , N_{BB} , and N_{AB} , respectively. Correspondingly, the binding energies of the atom pairs AA , BB and AB are denoted as V_{AA} , V_{BB} and V_{AB} . The coordination numbers (number of nearest-neighbors) in the two structures of interest here, the diamond structure (Si, Ge) and the fcc-structure of Ag and Cu, are $z = 4$ and $z = 12$, respectively. The variation of the energy due to mixing U_{mix} is

$$\begin{aligned} U_{\text{mix}} = & -(N_{AA} V_{AA} + N_{BB} V_{BB} + N_{AB} V_{AB}) \\ & + \frac{1}{2} (z N_A V_{AA} + z N_B V_{BB}). \end{aligned} \quad (2.6)$$

The sum of the first three terms is the energy after mixing and the sum of the last two terms is the energy before mixing. The factor $1/2$ occurs because there are $z/2$ bonds per atom. Note that the definitions of binding energy and internal energy imply an opposite sign: a higher binding energy

corresponds to a lower internal energy! The numbers of atom pairs N_{AA} , N_{BB} and N_{AB} can be expressed in terms of the concentrations

$$\begin{aligned} x_A &= N_A/N \\ x_B &= N_B/N \text{ with} \end{aligned} \quad (2.7)$$

$$N = N_A + N_B$$

and one obtains

$$\begin{aligned} N_{AA} &= N_A x_A z/2 = N x_A^2 z/2 \\ N_{BB} &= N_B x_B z/2 = N x_B^2 z/2 \\ N_{AB} &= N_A x_B z/2 = N x_A x_B z/2 . \end{aligned} \quad (2.8)$$

With that the energy of mixing U_{mix} becomes

$$U_{\text{mix}} = N z x_A x_B W_{AB} \quad (2.9)$$

with

$$W_{AB} = \frac{1}{2}(V_{AA} + V_{BB}) - V_{AB} . \quad (2.10)$$

If $W_{AB} < 0$ then the alloy has a higher binding energy and the internal energy of the alloy is lower than the sum of the internal energy of the constituents. Since $x_A + x_B = 1$ the energy of mixing has the form of a parabola.

$$U_{\text{mix}} = N z x_A (1 - x_A) W_{AB} . \quad (2.11)$$

Associated with a mixing of two components is always an enlargement of the entropy. This is because microscopically a mixture can be realized in many different ways. The different microscopic realizations originate from the exchange of atoms A with atoms B . The number of possibilities for an exchange of all atoms $N = N_A + N_B$ is $N!$. The exchange of atoms A and B among themselves, however, does not constitute a discernibly different microscopic state. The number of discernible states is thus $N!/(N_A! N_B!)$. With that the entropy of mixing becomes

$$S_{\text{mix}} = k \ln \frac{N!}{N_A! N_B!} = k \ln \frac{N!}{(N x_A)! (N x_B)!} . \quad (2.12)$$

With Stirling's approximation for large numbers $N \ln N! \approx N \ln N - N$, $N \gg 1$ one obtains

$$S_{\text{mix}} = -N k [x_B \ln x_B + (1 - x_B) \ln (1 - x_B)] . \quad (2.13)$$

The entropy S_{mix} is zero for $x_B = 0$ and $x_B = 1$ and positive for intermediate x_B . The free enthalpy of mixing is

$$\begin{aligned} G_{\text{mix}} &= U_{\text{mix}} - T S_{\text{mix}} \\ &= N \{ z x_B (1 - x_B) W_{AB} + k T [x_B \ln x_B + (1 - x_B) \ln (1 - x_B)] \} . \end{aligned} \quad (2.14)$$

The function has an extreme at $x_B = 0.5$. Whether it is a minimum or a maximum depends on the ratio of W_{AB} and $k_B T$. One has

$$\text{a minimum for } z W_{AB}/k_B T < 0.5, \quad (2.15)$$

$$\text{a maximum for } z W_{AB}/k_B T > 0.5. \quad (2.16)$$

Examples for $z W_{AB}/k_B T = 0.5$, 2.5 and 3 are displayed in Fig. 2.16. For negative values of W_{AB} the free enthalpy of mixing is always smaller than the sum of the free enthalpies of the separate components. In that case the alloy is continuously miscible. The same holds for any system, only if the temperature is high enough (2.14). The system becomes unstable if the free enthalpy has a maximum at $x_B = 0.5$. It decomposes into two separate phases, one with a concentration of the B -component $x'_B < 1/2$ and the other one with $x''_B > 1/2$. This is independent of the sign of the free enthalpy of mixing. For the special case when $G_{\text{mix}}(x_B)$ is symmetric around $x_B = 1/2$ (Fig. 2.16) it is easy to see that the instability exists not only at $x_B = 1/2$ but in the entire range between the two minima of $G_{\text{mix}}(x_B)$. Figure 2.17 displays the more general case of an asymmetric shape of $G_{\text{mix}}(x_B)$. The two concentrations x'_B and x''_B of the two phases into which the system separates are determined by the condition that the system as a whole must remain in equilibrium, that is, the chemical potentials of the two phases must be equal. The chemical potentials of the atoms of type B in the two phases are

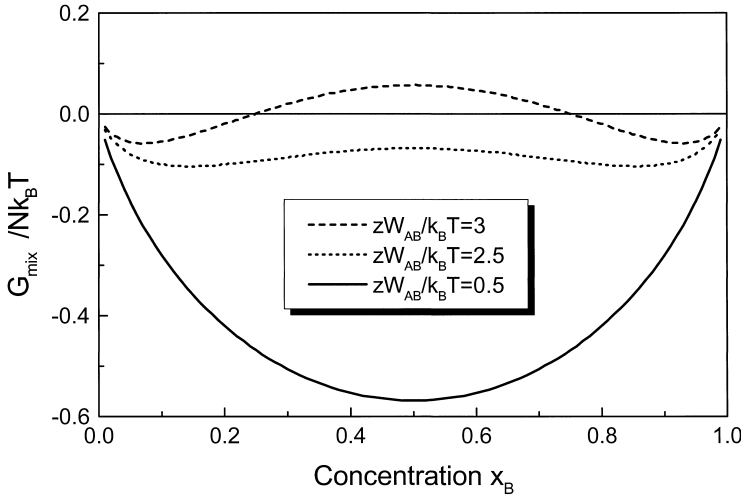


Fig. 2.16. The free enthalpy of a solid mixture according to a simple model (2.14). The solid line corresponds to the limiting case in which an intermediate maximum is not yet present. If an intermediate maximum occurs, the system is unstable against phase separation into two phases, one depleted of N_B atoms and one enriched with N_B atoms. Phase separation occurs independent of whether the enthalpy of mixing is gained in the alloying process (dotted line) or not (dashed line for concentrations around 0.5)

$$\mu'_B = \frac{\partial G'}{\partial N_B} = \frac{1}{N} \frac{\partial G'}{\partial x_B} \quad (2.17)$$

$$\mu''_B = \frac{\partial G''}{\partial N_B} = \frac{1}{N} \frac{\partial G''}{\partial x_B} .$$

Hence the system decomposes into two phases for which the slope of the free enthalpy (Fig. 2.17) is equal. Of all (the infinite number of) points on the curve $G(x_B)$ that fulfil the condition of an equal slope the total free enthalpy is minimal for the particular pair of concentrations x'_B and x''_B through which a common tangent to $G(x_B)$ can be drawn. This common tangent condition uniquely determines the two concentrations and x'_B and x''_B . A few simple geometrical considerations demonstrate that the system indeed separates into two phases with concentrations x'_B and x''_B , and that an alloy is unstable in the entire concentration range between x'_B and x''_B . Consider an arbitrary intermediate concentration x_{B0} . Conservation of mass during the process of phase separation requires that the numbers of B-atoms in the two phases $N'_B = N'x'_B$ and $N''_B = N''x''_B$ obey the relation

$$N'x'_B + N''x''_B = (N' + N'')x_{B0} . \quad (2.18)$$

The ratio of the total number of atoms in the two phases becomes therefore equal to the ratio of the concentration differences

$$\frac{N'}{N''} = \frac{x''_B - x_{B0}}{x_{B0} - x'_B} . \quad (2.19)$$

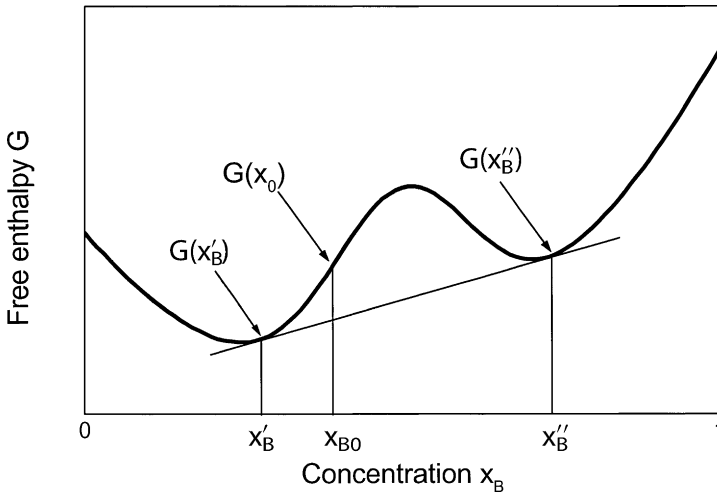


Fig. 2.17. Free enthalpy of an alloy with an intermediate maximum and two minima of a different depth. The system is unstable in the concentration range between the two points of tangency at x'_B and x''_B , and the system separates into two phases with the concentrations x'_B and x''_B . The free enthalpy of the two-phase system is described by the common tangent

A corresponding relation holds for the component A . This simple relation resembles the lever principle in mechanics and is therefore known as the lever rule of phase diagrams. It holds for any phase separation, regardless of its nature. After phase separation the free enthalpy of the system becomes

$$G(x'_B, x''_B) = G(x'_B) N'/N + G(x''_B) N''/N. \quad (2.20)$$

By substituting (2.20) into (2.19) and after a suitable rearrangement the enthalpy can be written as

$$G(x'_B, x''_B) = G(x'_B) + [G(x''_B) - G(x'_B)] \frac{x_{B0} - x'_B}{x''_B - x'_B}, \quad (2.21)$$

which is precisely the equation describing the y -coordinate in x_0 of the common tangent. Thus, the common tangent is simply the free enthalpy after phase separation. Between x'_B and x''_B all values of the common tangent are below the free enthalpy of the system before phase separation (Fig. 2.17). The system is therefore unstable with respect to phase separation in the entire gap between x'_B and x''_B . In the context of binary alloys this gap is known as the *miscibility gap*. As can be seen from the phase diagram (Fig. 2.15) a miscibility gap does exist for the Ag/Cu alloy. If a melt of 40 atom% silver and 60 atom% copper is cooled below the temperature of solidification, the solid crystallizes in the β -phase containing about 95% Cu. The remaining melt becomes enriched with Ag, until the Cu-rich α -phase (95.1% Cu) and the silver-rich β -phase (85.9% Ag) solidify together at the so-called eutectic point, which corresponds to 39.9% Cu in the melt at a temperature of 779°C. Upon further cooling the concentrations of the two solid phases should continue to vary in principle (Fig. 2.15). However, the equilibrium state can be achieved only for an extremely low cooling rate because of the low diffusivity of atoms in the solid phase. The concentrations in the darker and lighter areas in Fig. 2.15 therefore practically correspond to the equilibrium concentrations of the α - and β -phase at the eutectic point.

Thermodynamic reasoning can also be applied to the phase transition between the liquid and the solid phase in the case of a completely miscible alloy. Consider the free enthalpy of such a system in the liquid and solid phases (Fig. 2.18). The system is completely miscible since the free enthalpy is now represented by a function with a positive curvature in the entire concentration range. Liquid and solid phases coexist if the minima of the free enthalpies for the liquid and the solid state occur at different concentrations which is generally the case. The curves in Fig. 2.19 approximately represent the system Ge/Si. We consider first a high temperature $T > 1412^\circ\text{C}$. There, the free enthalpy of the melt is below that of the solid for all concentrations. This is because of the entropic contribution to the free enthalpy. At high temperatures, the entropy of the liquid phase is higher than that of the solid phase. The reason is that a liquid has more states of low quantum energy

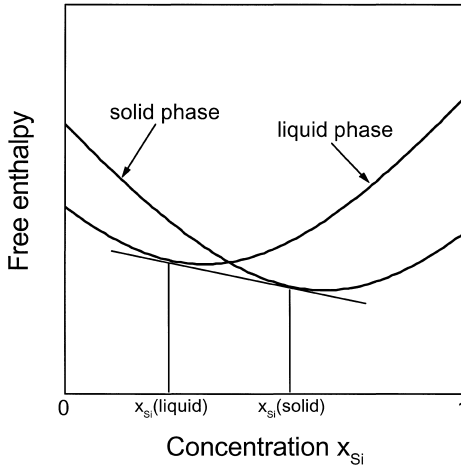


Fig. 2.18. Free enthalpy of the solid and liquid phase of a completely miscible alloy in the temperature range between the liquidus and solidus curves (schematic)

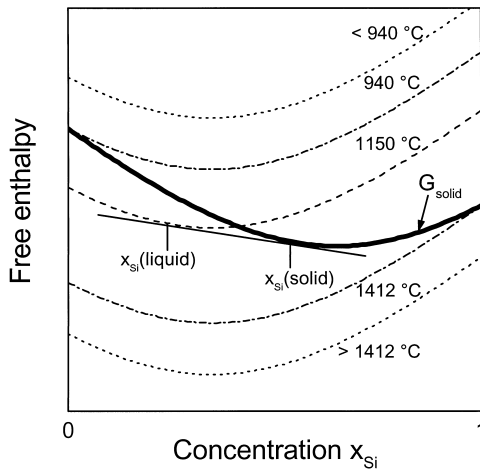


Fig. 2.19. Free enthalpies for the system Ge/Si at different temperatures as a function of the Si-concentration x_{Si} (schematic)

than a solid. Simply speaking, the degrees of freedom of the transverse sound waves of the solid become free translations in the melt. At a temperature of 1412°C the free enthalpies of the melt and the solid become equal for the concentration $x_{\text{Si}} = 1$. Melt and the solid coexist: we have reached the melting point of pure silicon. For even lower temperatures, e.g. at 1150°C , one has, according to the common tangent construction, a coexistence of a Si-depleted, liquid phase with a Si-enriched solid phase. Below 940°C finally, only the solid phase exists for all mixing ratios. If the cooling process is performed using a melt with a mixing ratio of 50 atom% Ge and 50 atom% Si, e.g., crystallites with 80% Si will solidify first at a temperature of about 1270°C . In the temperature range between the liquidus and solidus curve the equilibrium concentrations of Si in the

liquid and the solid state are given by the corresponding values for the concentrations of the liquidus and solidus curves. The ratio of the atom numbers in the two phases obey the lever rule (2.19). With decreasing temperature the solidified fraction of the melt increases, and the Si-concentration in the crystalline phase decreases. It is therefore not possible for continuously miscible alloys to grow a crystal out of a melt that has a homogeneous concentration ratio, unless one confines the crystallization to a small fraction of the melt.

One can utilize, however, the different equilibrium concentrations in the melt and the solid to purify a crystal of undesirable impurities. This is the basis of purification by zone melting: One begins by melting a narrow zone of a crystal rod at one end. In this molten zone the impurity concentration necessarily is as it was in the solid. Then, the molten zone is slowly pulled over the rod. If the liquidus and solidus curves are as in Fig. 2.14 with regard to an impurity (with Si as the base material and Ge as an impurity) then the re-crystallized rod in the cooling zone has a lower concentration of impurities than the (respective) melt. Hence, the impurities are enriched at that end of the rod that is molten last. A large section of the crystal can very effectively be purged of impurities by repeating the process many times.

2.7 Defects in Solids

Mechanical and electrical properties of solids are largely controlled by defects in the periodic structure. This section briefly reviews various known defects. In the previous section we have already learned about a special defect: In a diluted substitutional alloy, minority atoms may assume the sites of the majority atoms. In the context of semiconductors replacing majority atoms by atoms of another kind, preferably by atoms of a higher or lower valence is known as “doping”. Doping varies the electrical conductivity of a semiconductor by many orders of magnitude (see Sect. 12.3). Defects consisting only of one or a few atoms, as in the case of doping, are known as *point defects*. Point defects do not necessarily involve foreign atoms. The so-called *Frenkel defect* consists of an atom displaced from its regular site to an *interstitial* site. The atom in the interstitial site and the vacancy in the regular site together are named “Frenkel pair”. Since the bond energy of the atom is lower at the interstitial site the formation of a Frenkel pair requires energy. Nevertheless, Frenkel pairs do exist in equilibrium at higher temperatures because the formation of a Frenkel pair increases the entropy. That increase arises from the fact that the atom as well as the vacancy may sit in any possible interstitial or lattice site, respectively, thereby enjoying many distinguishable microscopic realizations. The number of possibilities to distribute n_v vacancies on N regular atom sites is $N!/[n_v!(N-n_v)!]$. Similarly, the number of possibilities to

distribute n_{int} interstitial atoms on N' interstitial sites is $N'!/[n_{\text{int}}!(N'-n_{\text{int}})!]$. For a Frenkel pair the number of interstitial atoms n_{int} necessarily equals the number of vacancies n_v . With $n = n_{\text{int}} = n_v$ one obtains for the entropy S (comp. 2.12)

$$\begin{aligned} S &= k \ln \frac{N!}{n!(N-n)!} + k \ln \frac{N'!}{n!(N'-n)!} \\ &\cong k [N \ln N + N' \ln N' - 2n \ln n - (N-n) \ln (N-n) \\ &\quad - (N'-n) \ln (N'-n)] . \end{aligned} \quad (2.22)$$

In equilibrium the system is in the state of lowest free energy $F = n\Delta E - TS$, in which ΔE is the energy required to create a Frenkel pair. The corresponding equilibrium concentration $\langle n \rangle$ is obtained by differentiating the free energy with respect to n

$$\frac{dF}{dn} = 0 = \Delta E + kT \ln \frac{\langle n \rangle^2}{(N' - \langle n \rangle)(N - \langle n \rangle)} . \quad (2.23)$$

Since the concentration of defects is small ($\langle n \rangle \ll N, N'$) $\langle n \rangle$ is approximately

$$\langle n \rangle \cong \sqrt{NN'} e^{-\Delta E/2kT} . \quad (2.24)$$

Hence, the concentration rises exponentially with the temperature according to an Arrhenius law. The activation energy in the Arrhenius law is half the energy required for the creation of a Frenkel-pair. The factor of two in the denominator of the exponent arises because vacancies as well as interstitial atoms are distributed independently in the crystal. One therefore has two independent contributions to the entropy. If the atom that is displaced from the regular site diffuses to the surface or into an interface ("Schottky defect"), the full energy of creation for the defect appears in the Arrhenius law. The reason is that for a macroscopic solid the number of available sites on the surface or in an interface are infinitely small compared to the number of sites in the bulk. In that case only the vacancies in the regular crystal sites contribute to the entropy.

Defects of the next higher dimension are line defects. A common intrinsic line defect is the *dislocation*. A simple example is shown in Fig. 2.20, which displays a cross section of a crystal with a dislocation. Around the core of the dislocation atoms are displaced from their regular lattice positions because of the elastic stresses. Most of the energy required to create a dislocation is actually in the elastic strain that decays rather slowly as one moves away from the core. Dislocations are described by the *Burgers vector*. The Burgers vector is constructed by considering the positions of atoms after completing a closed loop of an arbitrary size around the dislocation core for a lattice with and without a dislocation (Fig. 2.20). If the Burgers vector is oriented perpendicular to the dislocation line as in Fig. 2.20, the

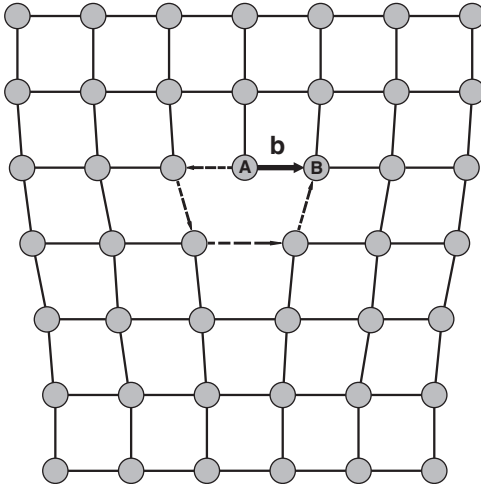


Fig. 2.20. Sectional drawing of a crystal with an edge dislocation (schematic). The dashed line represents a loop around the core of the dislocation. The loop begins with atom *A*. It would close at atom *B* if the dislocation were not present. The Burgers vector ***b*** points from atom *A* to atom *B*. The same Burgers vector is obtained for any arbitrary loop that encloses the dislocation

dislocation is called an “*edge dislocation*”. If the Burgers vector is oriented along the dislocation line, then the dislocation is called a “*screw dislocation*”, since by moving along a closed loop around the dislocation one climbs from one lattice plane onto the next. Edge dislocations and screw dislocations represent two limiting cases of a general, intermediate form of a dislocation. Furthermore, the angle between the orientation of the Burgers vector and the dislocation line may vary as one moves along the dislocation line. The modulus of the Burgers vector is equal to the distance of an atom plane for the common screw or edge dislocations. However, dislocations for which the modulus of the Burgers vector is only a fraction of a distance between an atom plane also exist. Such a *partial dislocation* is generated, e.g., if all atoms in a section of an fcc-crystal are displaced along a direction in a densely packed plane so as to produce a stacking fault (Fig. 2.9).

Dislocations play a crucial role in plastic deformation of crystalline material. Consider a shear force acting parallel to an atom plane. It is not feasible to make all the atoms glide simultaneously since the shear force works against the atomic bonds of all atoms in the glide plane at once. A step wise glide is energetically much more favorable. Firstly an edge dislocation is generated at the surface and then the dislocation is shifted through the crystal. Then gliding is effectuated by displacing the atoms row-by-row until the dislocation line has moved through the entire crystal. The required forces are much lower since fewer atoms are affected and bonds need not be broken but must merely be strained and re-oriented. Plastic deformations of a crystalline solid are therefore connected with the generation and wandering of dislocations. In a pure, ideally crystalline material dislocations can move easily, provided the temperature is not too low. For many metals,

e.g., room temperature suffices. Such materials have little resistance to plastic deformation. Examples are rods or wires consisting of annealed copper and silver. If the material is polycrystalline, e.g., after cold working, then the wandering of dislocations is hindered by the grain boundaries between the crystallites, and the material resists plastic deformation more effectively.

Problems

2.1 The phase transition from graphite to diamond requires high pressure and high temperature in order to shift the equilibrium in favor of diamond and also to overcome the large activation barrier. Suggest a method of producing diamond (layers) without the use of high pressure.

2.2 Below 910°C iron exists in the bcc structure (α -Fe). Between 910°C and 1390°C it adopts the fcc structure (γ -Fe). Assuming spherical atoms, determine the shape and size of the octahedral interstitial sites in γ -Fe ($a = 3.64 \text{ \AA}$) and in α -Fe ($a = 2.87 \text{ \AA}$). Sketch the lattices and the interstitial sites. For which phase would you expect the solubility of carbon to be higher? (Hint: The covalent radius of carbon is 0.77 \AA .) When molten iron containing a small amount of carbon ($\lesssim 1\%$) is cooled, it separates into a more-or-less ordered phase containing α -Fe with a small concentration of carbon atoms on interstitial sites (ferrite) and a phase containing iron carbide (cementite, Fe_3C). Why does this occur? Why does cementite strengthen the medium against plastic deformation?

(Hint: Fe_3C , like many carbides, is very hard and brittle.)

2.3 Copper and gold form a continuous solid solution with the copper and gold atoms statistically distributed on the sites of an fcc lattice. For what relative concentrations of copper and gold atoms do you expect ordered alloys and what would they look like? Draw the unit cells of these alloys and identify the corresponding Bravais lattices. Can you suggest an experiment which would determine whether the alloy is ordered or not?

2.4 Draw and describe the symmetry elements of all Bravais lattices.

2.5 Draw the primitive unit cell of the fcc lattice and determine the lengths of the primitive lattice vectors \mathbf{a}' , \mathbf{b}' , \mathbf{c}' (in units of the conventional lattice constant a) and also the angles α' , β' , γ' between the primitive lattice vectors. (Hint: Express the primitive lattice vectors as a linear combination of the lattice vectors \mathbf{a} , \mathbf{b} , \mathbf{c} of the face-centered cubic lattice and use elementary vector algebra.) What distinguishes this unit cell from that of the rhombic Bravais lattice?

2.6 Determine the ratio of the lattice constants c and a for a hexagonal close packed crystal structure and compare this with the values of c/a found for the following elements, all of which crystallize in the hcp structure: He ($c/a = 1.633$), Mg (1.623), Ti (1.586), Zn (1.861). What might explain the deviation from the ideal value?

2.7 Supposing the atoms to be rigid spheres, what fraction of space is filled by atoms in the primitive cubic, fcc, hcp, bcc, and diamond lattices?

2.8 Give a two-dimensional matrix representation of a 2-, 3-, 4-, and 6-fold rotation. Which representation is reducible?

2.9 Show that the rhombohedral translation lattice in Fig. 2.3 is equivalent to a hexagonal lattice with two atoms on the main diagonal at a height of $c/3$ and $2c/3$. Hint: Consider the projection of a rhombohedral translation lattice along the main diagonal into the plane perpendicular to this main diagonal. The main diagonal of the rhombohedral lattice is parallel to the c -axis of the hexagonal lattice. How are the a and the c axis of the corresponding hexagonal lattice related to the angle $\alpha = \beta = \gamma$ and the length $a = b = c$ of the rhombohedral lattice?

2.10 Take a piece of copper wire and anneal it by using a torch! Demonstrate that the wire is easily plastically deformed. Then pull the wire hard and suddenly or work it cold using a hammer. How is the plastic behavior now? Explain the observations!



<http://www.springer.com/978-3-540-93803-3>

Solid-State Physics

An Introduction to Principles of Materials Science

Ibach, H.; Lüth, H.

2009, XIV, 536 p., Softcover

ISBN: 978-3-540-93803-3